The Conformational Behavior of Novel Glycosidase Inhibitors with Substituted Azepan Structures: An NMR and Modeling Study

Karina Martínez-Mayorga,[a] José L. Medina-Franco,[a] Silvia Mari,[a] F. Javier Cañada,[a] Eliazar Rodríguez-García,[c] Pierre Vogel,[c] Hongqing Li,[b] Yves Blériot,*[b] Pierre Sinaÿ,*[b] and Jesús Jiménez-Barbero*[a]

Dedicated to Prof. Dr. Pedro Molina on the occasion of his 60th birthday

Keywords: Conformational analysis / Nuclear magnetic resonance / Polyhydroxyazepanes / Molecular modeling / Glycosidase inhibitors / Glycomimetics

The conformational analysis of a series of configurational isomers of 2-(hydroxymethyl)azepan-3,4,5,6-tetrols **1**–**4** has been carried out. ^{1}H NMR spectroscopic data, especially vicinal *J* couplings and nuclear Overhauser enhancements (NOE), assisted by molecular mechanics, molecular dynamics and Monte Carlo calculations, have been used. A fairly good agreement between experimental and calculated data has been found. The different isomers exist in a conformational equilibrium between two chair-like structures. TR-NOE experiments have also allowed us to demonstrate that the bound conformation of compound **2** to the β-glucosidase from almonds is the major one of this compound present in solution. Finally, molecular docking of the different conformations of these compounds in the binding site of three different enzymes has been performed in order to try to rationalize the observed inhibition of these molecules.

Introduction

The quest for glycosidase inhibitors has been the subject of extensive research in the past few years due to their potential use as therapeutic agents.[1] Indeed, several molecules with this capacity have been shown to interact with receptors related to diabetes,[2] Gaucher's disease,[3] HIV infection,[4] viral infections,[5] and even cancer.[6] Moreover, they have also been used as chemical probes, in combination with crystallography, modeling and other biochemical and biophysical methods, to provide new insights into the glycosidase mechanism[7] and they are now expected to find an increasing number of applications as beneficial drugs.[8]

We have recently reported the synthesis and biological evaluation of a variety of azepan derivatives with four hydroxy groups attached to the ring,[9] as well as a hydroxymethyl moiety (Figure 1), which mimic monosaccharides with different stereochemistries, that is, α-D-*gluco* (**1**), β-L-*ido* (**2**), β-D-*manno* (**3**), and α-L-*gulo* (**4**). These compounds were shown to behave as moderate to good glycosidase inhibitors with **1** and **3** inhibiting bovine liver β-galactosidase

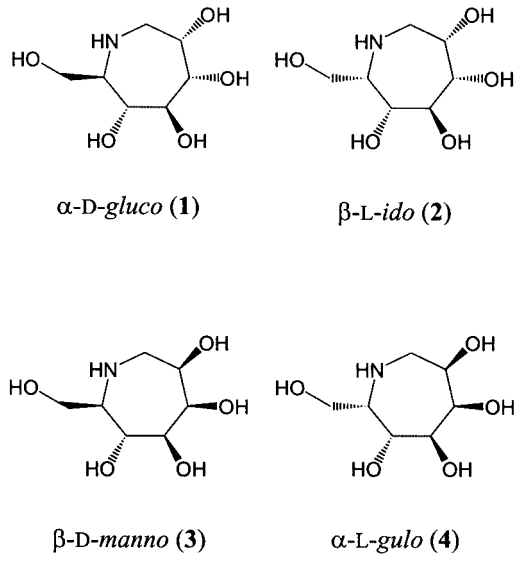

Figure 1. Schematic view of compounds **1**−**4**

[a] Centro de Investigaciones Biologicas, CSIC,
Ramiro de Maeztu 9, 28040 Madrid, Spain
E-mail: jjbarbero@cib.csic.es
[b] Ecole Normale Supérieure, Département de Chimie, UMR 8642,
24 rue Lhomond, 75231, Paris Cedex 05, France
[c] Institute of Glycochemistry and Asymmetric Synthesis, Swiss Federal Institute of Technology (EPFL), BCH,
1015 Lausanne, Switzerland
Supporting information for this article is available on the WWW under http://www.eurjoc.org or from the author.

and coffee bean α-galactosidase in the low micromolar range, respectively, despite showing *gluco*- and *manno*-like configurations.[9]

On this basis, and in order to try to clarify the structural basis for this behavior, we now report on the conformational study of these seven-membered ring compounds by using a NMR/modeling approach. These seven-membered ring systems, such as **1**−**4**, are inherently flexible and may assume several conformations that can interconvert with relative low energy barriers.

Proton magnetic resonance (^{1}H NMR) spectra have been recorded at neutral and acidic pH, the corresponding coupling constants have been deduced, and nuclear Overhauser effect (NOE) experiments have been evaluated for **1**−**3**. These data along with the results from molecular mechanics, molecular dynamics, and Monte Carlo calculations[10] have permitted us to evaluate the conformational behavior of these iminoalditols. In a further step, STD[11] (Saturation Transfer Difference) and TRNOE[12] experiments have been carried out to deduce the conformation of **3** bound to β-glucosidase from almonds. Finally, molecular docking studies[13] of these molecules have been carried out in order to characterize their binding mode to three different glycosidase enzymes[14] and to try to rationalize the ability of **1**−**4** to behave as gluco- and galactosidase inhibitors.

Methods

Materials: The synthesis of these molecules has been published elsewhere.[9]

NMR: Proton assignments were performed using standard 1D, 2D-COSY, NOESY, and HSQC experiments.[15] The coupling constants for **1**−**3** were obtained from ^{1}H NMR spectra recorded in acidic media; additional experiments were carried out under neutral conditions for β-L-*ido* (**2**) and α-D-*gluco* (**1**). Proton−proton interatomic distances were estimated from the enhancements measured by selective 1D NOE experiments, with the DPFGSE NOE sequence proposed by Shaka and co-workers.[16]

Molecular Modeling: Molecular mechanics (MM), molecular dynamics (MD) and Monte Carlo (MC) studies[17] were conducted with the MACROMODEL program, version 5.5.[18] Both the AMBER*[19] and MM3*[20] force fields were used. The energies were minimized by using the PR conjugate gradient method. A bulk dielectric constant of 80 was used when calculations were performed ''in vacuo''. The GB/SA (Generalized Born Surface Area) solvation model[21] was also used. The starting coordinates for dynamics calculations were those obtained after energy minimizations. Simulations were carried out over 2 ns at 300 K. Monte Carlo studies were conducted by using default parameters implemented in MACROMODEL; 300 trial structures were generated for each molecule. Coupling constants were calculated by using the empirical Karplus equation proposed by Haasnoot et al.[22] Interatomic H−H distances and estimated NOEs were calculated by using the NOEPROM program, which is available from the authors upon request.[23]

Docking simulations were conducted with AutoDock 3.0.[24] X-ray coordinates for the enzymes were taken form the Protein Data Bank or other work.[25−27] This program performs automated docking of the whole ligand with user-specified dihedral flexibility within a rigid protein binding site. Before docking, ligands as well as all water molecules were removed except for the putative catalytic water molecule of the glucoamylase. Docking studies with β-glucosidase were conducted with the B chain. Polar hydrogen atoms were added by using the auxiliary program Auto Dock Tools. Energies were evaluated from precalculated grids with molecular affinity potentials. Affinity grid files were generated using the auxiliary program Autogrid. The centers of the coordinates of the crystal ligands were taken as the centers of the grids, and the dimensions of the grids were 23 × 23 × 23 Å with points separated by 0.375 Å.

The possible conformations of the analogues (see below) were protonated at the nitrogen atom and minimized with the AMBER* force field and the PR conjugate gradient method. The dielectric constant was set to 80. Gasteiger charges were computed with the auxiliary program Auto Dock Tools and nonpolar hydrogens merged. AutoDock randomized the initial position.

With α-galactosidase and glucoamylase, the configurational and translational exploration was conducted with a Monte Carlo simulated annealing technique. With β-glucosidase, the Lamarckian Genetic Algorithm implemented in the program was used. For each starting structure a total of 100 independent Monte Carlo or genetic algorithm simulations were made. For each Monte Carlo simulation there were 50 constant temperature cycles with a maximum of 3000 steps accepted or rejected. The initial temperature was RT = 1000 cal·mol^{-1} and was reduced by a factor of 0.95 each cycle. All the other values for the Monte Carlo simulations as well as Lamarckian genetic algorithm search parameters were taken from the default values of AutoDock.

After docking, the 100 solutions were clustered into groups with RMS deviations less than 1.0 Å. The clusters were ranked on the basis of the lowest energy representative of each cluster. Note that the AutoDock energies as reported here may not represent the true energies, rather they are just a measure of the scoring function used.

Results and Discussion

The conformational analysis of the different molecules was performed by using a combination of experimental NMR spectroscopic data, assisted by modeling methods. The analysis of the shapes of seven-membered rings is challenging and a variety of forms may occur. The substitution of different carbon atoms by hydroxy groups, with different stereochemistries, and, moreover, by a bulky hydroxymethyl moiety must obviously modify the set of conformations that are accessible. The conformation of the seven-membered ring as well as of that of the hydroxymethyl group were explored.[28] In all cases, the NMR spectrum obtained under acidic conditions was of higher quality than the one

recorded under neutral conditions and allowed a more precise measure of the key *J* and NOE parameters.

α-D-*gluco*-Like Compound 1

The experimental vicinal proton−proton coupling constants and NOE enhancements (from which interatomic H−H distances may be estimated) are shown in Table 1 and 2, respectively. Molecular mechanics, dynamics and Monte Carlo calculations predicted the existence of two major conformations, dubbed **A1** and **B1** (Figure 2), although with some flexibility around the conformers depicted in the figures. Conformer **B1** is about 5.6 kJ·mol^{-1} more stable than **A1** according to the AMBER* force field and the GB/SA solvent model. Similar results in terms of energies and geometries were obtained when either a bulk dielectric constant (ε = 80) or when the MM3* force field was employed. The bulk hydroxymethyl group (C7) is attached to C6 in the more stable pseudoequatorial orientation in both conformers. For simplicity, and as sugar mimics, the chosen numbering is related to the sugar nomenclature, with the deoxy position of **1**−**4** being C-1. The hydroxy groups at positions 3, 4, and 5 of conformer **B1** are also equatorially oriented, while OH-2 has a pseudoaxial disposition. In contrast, the OH-3 of conformer **A1** is the only hydroxy group that assumes a relative pseudoaxial orientation. Table 1 also gives the AMBER*-computed proton−proton dihedral angles for **A1** and **B1**, along with the estimated couplings. Table 2 shows the AMBER*-MM/MD predicted average interatomic distances, along with the expected NOEs. It may be observed that conformers **A1** and **B1** may be differentiated on the basis of the expected couplings for $J_{1,2}$ and $J_{3,4}$. Indeed, the experimental data seem to indicate that **B1** is predominant (Table 1) although with some contribution from **A1**-type conformers. The experimental couplings for the vicinal ring proton pairs can be explained using the same rationale. According to the data, similar conformational equilibria are seen at neutral and acidic pH.

Table 1. Experimental and expected $^3J_{H,H}$ and estimated torsion angles (τ) for the α-D-*gluco*-like derivative **1**

$^3J_{H,H}$	Experimental $^3J_{H,H}$ (Hz)		Expected (MM/MD/MC) Conformer **B1**		Conformer **A1**	
	Neutral pH	Acidic pH	τ (°)	*J* (Hz)	τ (°)	*J* (Hz)
$J_{1',2}$	< 1.5	< 1.5	69.5	1.0	86.3	1.6
$J_{1,2}$	6.0	6.0	48.8	5.0	154.3	9.7
$J_{2,3}$	4.4	4.4	52.6	3.1	41.8	4.5
$J_{3,4}$	8.0 ± 0.5	9.2	175.4	10.0	153.3	6.4
$J_{4,5}$	9.1	9.1	160.4	9.7	160.9	9.7
$J_{5,6}$	8.7	8.7	160.1	8.6	171.1	10.3

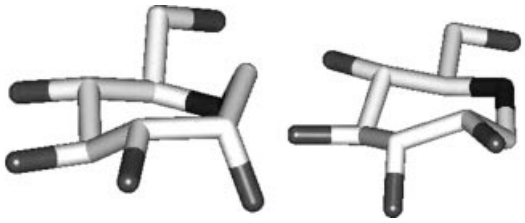

Figure 2. Conformations **A1** (right) and **B1** (left) of α-D-*gluco*-like analogue **1** (AMBER*; ε = 80)

Similar conclusions are reached from the interatomic distances. In this case, key differences between the two calculated conformations are found for the H1′−H3 and H2−H5 proton pairs. Again, the experimental NOEs suggest a major contribution from **B1**-type conformers, since the H1′−H3 cross-peak displays an appreciable intensity and the H2−H5 cross-peak intensity is just above the noise level, in contrast to what is expected for the **A1**-type geometry. The average distances and NOE values obtained from the MD calculations are in all cases in between those values predicted for the single **A1** and **B1** conformers and are also in agreement with the observed data. Thus, the MD trajectory seems to provide a reasonable estimate of the conformational distribution (Table 2). Indeed, several reversible transitions between the **A1** and **B1** forms (Supporting Information, see also the footnote on the first page of this article) take place during the simulation, which also indicates that the energy barrier for interconversion should be relatively low.

Table 2. Experimental and calculated NOEs and H−H distances for α-D-*gluco*-like derivative **1**

Proton pair	Experimental NOE		Molecular modeling MM (*r*)		MD	
	Intensity[a]	Upper limit distance[b]	Conformer **A1**	Conformer **B1**	$\langle r^{-6}\rangle^{-1/6}$	NOE intensity[c]
1′–2	ms	2.8	2.6	2.5	2.6	6.6
1–2	m	2.9	3.0	2.4	2.8	3.7
1′–3	mw	3.1	4.2	2.6	3.2	1.3
1′–5	w	3.5	4.2	2.4	3.2	1.5
2–3	s	2.6	2.3	2.4	2.4	9.7
2–5	vw	4.0	2.4	3.9	2.7	4.2
3–4	m	2.9	3.0	3.1	3.1	2.1
3–5	ms	2.8	2.8	2.3	2.7	4.8
4–5	m	2.9	3.0	3.0	3.1	2.0
4–6	s	2.6	2.3	2.7	2.5	8.3
5–6	mw	3.1	3.0	3.0	3.1	1.9

[a] Average of those obtained at different mixing times. s: strong; ms: medium strong; m: medium; mw: medium weak; w: weak; vw: very weak. [b] Upper limits of distances (Å) are provided, according to the observed intensities, as 2.6, 2.8, 2.9, 3.1, 3.3, 3.5 Å. [c] NOE intensities calculated with NOEPROM (%).

Regarding the rotamer distribution around the C6−C7 linkage of the hydroxymethyl group, Table 3 gives the expected coupling values for the three possible staggered rotamers and also the experimental data for comparison. The conformers were dubbed *gg*, *gt*, and *tg*, following the currently used nomenclature for sugars. The GB/SA AMBER* calculations predicted small energy differences between the three rotamers (less than 3 kJ·mol^{-1}), *gt* being the most populated one. However, the observed results, with one small and one medium coupling constant value, indicate that a rotational equilibrium between the *gg* and the *gt* rotamers occurs, with a similar population of both forms. Similar behavior has been described for Glc/Man pyranose rings, since in these cases, the equatorially oriented O4 in the six-membered chair of Glc/Man precludes the existence of the *tg* rotamer displaying destabilizing O1−O3 interactions. The results obtained at neutral and acidic pH are very similar, which indicates the same type of equilibrium exist under both experimental conditions. Thus, the state of protonation of the nitrogen atom does not seem to influence the conformational distribution at the C6−C7 torsion, as also observed for the seven-membered ring itself (see also Table 1).

Table 3. Experimental and expected coupling constants (Hz) [from the proton−proton torsion angles, in brackets (°)] for the three staggered rotamers of the hydroxymethyl group of α-D-*gluco*-like compound **1**; the geometry of the **B1** conformer was employed

		Exp. NMR	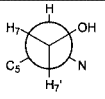 *gt*	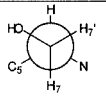 *tg*	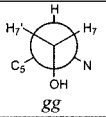 *gg*
ΔE (kJ/mol)[a]			0.0	1.8	2.8
$^3J_{H\text{-}H}$ (τ)	6-7	2.0	3.7 (60.5)	10.9 (177.4)	2.5 (59.1)
	6-7'	6.5	10.9 (179.3)	4.1 (62.8)	1.6 (59.6)

[a] Calculated with AMBER*; GB/SA.

β-L-*ido*-Like Compound 2

Compound 2 differs from 1 by the stereochemistry at position C6, to which the C7 hydroxymethyl group is attached. The experimental and calculated coupling constants are given in Table 4, while the corresponding NOE-based information is gathered in Table 5. Again, only the results obtained by using AMBER* and GB/SA are shown, since those with MM3* and a bulk dielectric constant of 80 are very similar.

Table 4. Experimental and expected $^3J_{H,H}$ and estimated torsion angles (τ) for the β-L-*ido*-like derivative **2**

$^3J_{H,H}$	Experimental $^3J_{H,H}$ (Hz)		Expected (MM/MD/MC) Conformation **A2**		Conformation **C2**	
	Neutral pH	Acidic pH	τ (°)	*J* (Hz)	τ (°)	*J* (Hz)
$J_{1',2}$	< 1.5	2.5	83.6	1.8	65.0	1.2
$J_{1,2}$	6.0	6.5	160.3	10.3	53.1	4.4
$J_{2,3}$	< 1.5	1.5	42.4	4.3	78.0	1.0
$J_{3,4}$	7.0	6.3	147.3	5.4	161.6	7.7
$J_{4,5}$	3.0	2.8	165.4	10.0	91.0	0.7
$J_{5,6}$	< 1.5	< 1.0	63.5	3.2	80.0	0.4

The Monte Carlo search followed by minimization produced two stable conformations of the β-L-*ido*-like compound **2**. One of them, named **A2** had a very similar geometry to that described above as **A1** for the α-D-*gluco*-like derivative **1**. The second one was not exactly like **B1**, but somehow distorted, probably due to the different stereochemistry at C6, and was dubbed **C2** (Figure 3). This was the global minimum, stabilized with respect to **A2** by 12.5 kJ·mol^{-1}. The conformational equilibrium was evaluated as above. From the coupling values, key differences between the conformers are expected for $J_{1,2}$, $J_{2,3}$ and $J_{4,5}$ (Table 4). It is evident that the observed values are between those expected for **A2** and **C2**. From the NOE data, the major proton−proton interatomic distance differences occur for the H1′−H3, H1′−H6 and H3−H6 proton pairs (Table 5). Therefore, a conformational equilibrium between **A2** and **C2** is evident, **C2** being predominant. By comparing the major conformers of α-D-*gluco* (**1**) and β-L-*ido* (**2**), **B1** and **C2**, respectively, we can assume that the difference is due to the necessity of the hydroxymethyl group to adopt a pseudoequatorial orientation, which cannot be accommodated by the **B1**-type geometry. Distortion of the ring **B** seen in **C** can be attributed to the different conformation at C6. Despite the relatively high predicted energy difference, which would preclude the existence of **A2**-type conformers, their presence is acknowledged due to the experimental observations. Moreover, MD simulations starting form either **A2** or **C2** gave rather stable trajectories with no interconversions, somehow proving the conformational stability of these geometries.

The conformation of the lateral C6−C7 chain was also analyzed. The highest relative energy of the three possible rotamers is ca. 4 kJ·mol^{-1} (from *gg* to *gt*, see Table 6). The coupling constants for the hydroxymethyl group of the three main rotamers are shown in Table 6. Following the reasoning used above for compound **1**, the two intermediate values obtained at neutral pH are in agreement with an almost 50:50 conformational distribution of the *gt* and *tg* rotamers, as expected for L-*ido*-type sugars, with essentially no contribution from the *gg* form. However, in this case, lowering the pH towards acidic conditions (pH = 4.5) influences the conformational distribution of the lateral chain. Indeed, the increase in one of the $J_{6,7}$ couplings (from 7 to 9 Hz) is in agreement with a change in the conformational distribution to a 75:25 ratio in favor of the *gt* rotamer.

β-D-*manno*-Like Compound 3

The experimental (at acidic pH) and calculated coupling constants of β-D-*manno*-like compound 3 are compared in Table 7. The difference between compounds 1 and 3 lies in the stereochemical differences at positions 2 and 3 (sugar-related nomenclature). In this case, again two conformers A3 and B3 were found by the MC protocol with very similar geometries to those found for 1. The main difference lies in the relative disposition of the substituents at C2 and C3 and in this case these groups are orientated differently. Thus, the OH-3 and OH-2 groups of conformer B3 are axially and equatorially oriented, respectively, while in con-

Table 5. Experimental and calculated NOEs and H−H interatomic distances for the β-L-*ido*-like derivative **2**

Proton pair	Experimental NOE		Molecular modeling		
	Intensity[a]	Upper limit distance	MM (r) Conformer **A2**	MM (r) Conformer **C2**	MD $\langle r^{-6}\rangle^{-1/6}$
1'–2	ms	2.8	2.6	2.5	2.5
1–2	ms	2.8	3.1	2.4	2.6
1'–3	m	2.9	4.2	2.4	3.1
1'–4	vw	4.0	4.1	4.5	4.4
1'–6	mw	3.1	4.1	2.4	3.0
2–3	s	2.6	2.3	2.6	2.5
2–4	vw	4.0	3.7	3.8	3.8
2–6	vw	4.0	3.8	4.0	3.9
3–4	mw	3.1	3.0	3.0	3.0
3–6	ms	2.8	4.9	2.3	3.1
4–5	ms	2.8	3.1	2.6	2.8
5–6	ms	2.8	2.5	2.6	2.6

[a] s: strong; ms: medium strong; m: medium; mw: medium weak; w: weak; vw: very weak.

Figure 3. Conformations **A2** (left) and **C2** (right) of β-L-*ido*-like analogue **2** (AMBER*; GB/SA)

Table 6. Experimental and expected coupling constants (Hz) [from the proton−proton torsion angles (°), in brackets] for the three staggered rotamers of the hydroxymethyl group of the β-L-*ido*-like compound **2**; the geometry of the major **C2** conformer was employed

	Experimental (neutral / acidic pH)	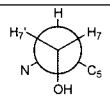 *gg*	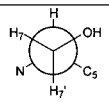 *gt*	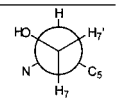 *tg*
ΔE (kJ/mol)[a]		0.0	4.2	2.7
$^3J_{H,H}$ (τ) 6-7	7.0 / 5.5	2.4 (59.2)	3.7 (65.9)	10.9 (179.5)
6-7'	7.0 / 9.0	1.6 (59.8)	10.7 (174.5)	3.7 (60.2)

[a] Calculated with AMBER*; GB/SA.

Table 7. Experimental and expected $^3J_{H,H}$ and estimated torsion angles (τ) for the β-D-*manno*-like derivative **3**

$^3J_{H,H}$	Experimental $^3J_{H,H}$ (Hz)	Expected (MM/MD/MC) Conformer **A3** τ (°)	*J* (Hz)	Conformer **B3** τ (°)	*J* (Hz)
$J_{1',2}$	7.0	38.5	6.4	154.5	8.9
$J_{1,2}$	5.5	79.9	0.9	35.8	7.9
$J_{2,3}$	< 1.5	32.2	5.5	81.7	0.8
$J_{3,4}$	< 1.5	41.7	4.6	66.5	1.6
$J_{4,5}$	8.5	158.2	9.8	172.2	8.9
$J_{5,6}$	9.0	173.2	10.3	166.4	10.1
$J_{6,7a}$	2.8	56.7	4.2	54.3	2.1
$J_{6,7b}$	7.0	11.1	11.1	65.1	1.9

former A3 the OH-3 and OH-2 groups are equatorially and axially oriented, respectively, with the hydroxymethyl group always adopting a pseudoequatorial orientation. The experimental data indicate the existence of a conformational equilibrium between A3 and B3 with the B form prevalent, as observed for 1 (Figure 4). Actually, the application of the MM/MD/MC protocols to β-D-*manno* (3) produced results remarkably similar to those for α-D-*gluco* (1).

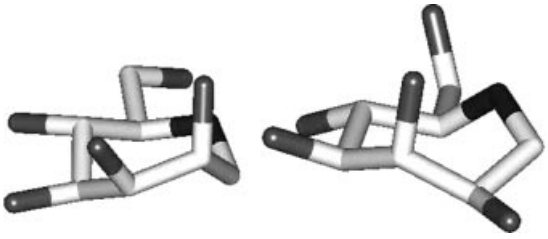

Figure 4. Conformations **A3** (left) and **B3** (right) for the β-D-*manno*-like analogue **3** (AMBER*; GB/SA)

The couplings for the hydroxymethyl group of **3** are shown in Table 7, while the reasoning can be followed with the Newman projections and the expected values for *gg*, *gt*, and *tg* rotamers given in Table 7. The observed values (2.8, 7.0 Hz) are in agreement with a *gg*−*gt* equilibrium similar to those predicted for Glc/Man pyranose analogues (see above for **1**), but with a higher predominance of *gt* rotamers than was the case with **1**.

α-L-*gulo*-Like Compound 4

The peaks in the ^{1}H NMR spectrum of **4** showed extensive overlapping at any pH, and it was not possible to unambiguously deduce the relevant *J* couplings and/or NOEs to account for the conformational distribution. However, the

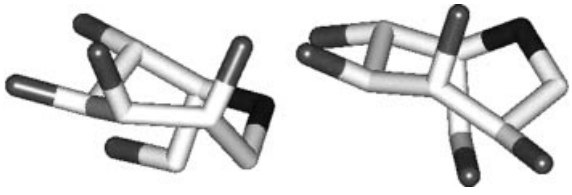

Figure 5. Conformations **A4** (right) and **B4** (left) for the α-L-*gulo*-like analogue **4** (AMBER*; GB/SA)

application of the modeling protocol also led to a participation of two chair-like forms, dubbed **A4** and **B4** (Figure 5), similar to those reported for **2**, with the **B4** conformer being the preferred one from the molecular mechanics calculations. Indeed two axial substituents may be observed for **A4**, namely the hydroxymethyl group and OH-2, while only OH-3 adopts an axial disposition in conformer **B4**.

Therefore, the conformational behavior of the four compounds can be described as a conformational equilibrium between two calculated chair-like conformations, with one being predominant. The hydroxymethyl substituent group can also adopt two conformations, with one predominating in some cases.

The Bound State

In a further step, we investigated the mode of binding of these molecules to glycosidase enzymes. NMR experiments have been shown to be useful for deducing the conformation of carbohydrate analogues bound to lectins, and in some cases, to enzymes. Thus, we performed TRNOE and STD experiments in order to study the complexes of **3** with bovine liver β-galactosidase and with the β-glucosidase from almonds. Unfortunately, it was not possible to obtain any NMR spectroscopic data for **3** bound to the former enzyme. Very probably, given the good inhibition ability of **3**, the kinetic features of the molecular recognition phenomenon are not suitable for the strict requirements of STD and TRNOE experiments. Fortunately, both STD and TRNOE experiments (Figure 6) permitted us to deduce some information as regards the binding of **3** to the β-glucosidase from almonds. The STD experiment shows that the major transfer of magnetization from the enzymic protons to the ligand involves H2, H3, H4, and to some extent H5 atoms, that is, one of the sides of the molecule.

Figure 6 allows the NOESY spectrum (mixing time 300 ms) of free **3** to be compared with the TRNOESY spectrum

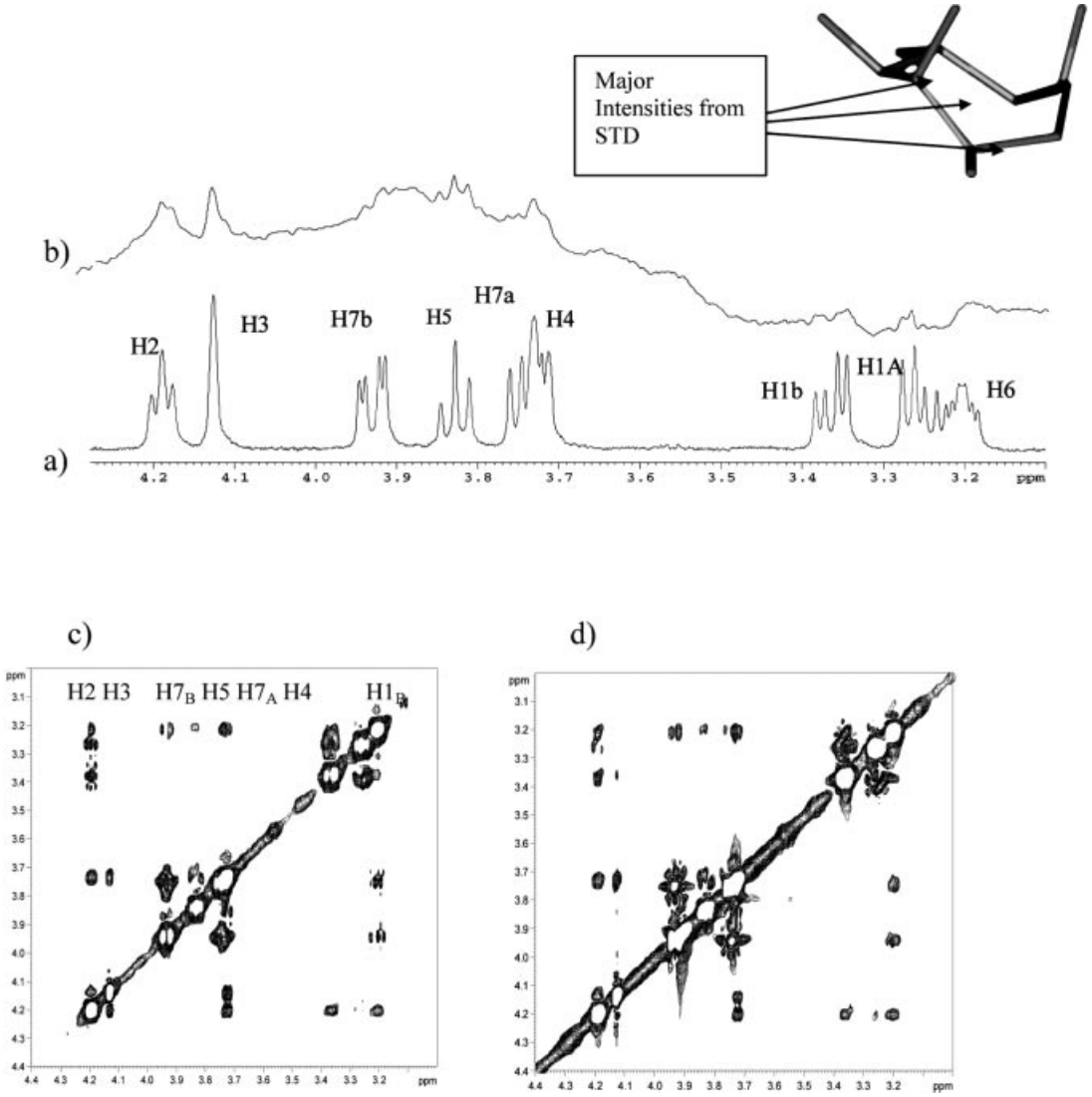

Figure 6. (a) ^{1}H NMR spectrum of the free ligand (1.5 mM) (50 mM in phosphate buffer, pH 5.8, and 25 °C); (b) ^{1}H NMR STD spectrum of the ligand (1.5 mM) bound to almond glucosidase (50 μM) (50 mM in phosphate buffer, pH 5.9, and 25 °C); NOE data for **3** in the free and enzyme-bound states: (c) NOESY (300 ms) of free **3**; (d) TRNOESY (150 ms) of **3** (1.5 mM) with almond glucosidase (50 μM)

of **3** (mixing time 150 ms) in the presence of the glucosidase (30:1 molar ratio). It is observed that despite some antiphase character in the cross peaks of the spectrum of the free molecule, as expected for a small molecule and a relatively short NOE mixing time, the set and pattern of the observed cross peaks are basically identical. This seems to indicate that very probably, the β-glucosidase from almonds recognizes **3** in its major conformation present in solution, that is **3B**.

Inhibition Experiments

The inhibition ability of these molecules towards several glycosidases has been demonstrated previously.[9] As shown below, docking experiments enabled us to predict the relative inhibitory ability of these compounds. In order to test whether this protocol (NMR, molecular mechanics + docking) could be extended to other glycosidases, the inhibition abilities of **1**−**4** towards two additional glucosidases were evaluated and the percentages of inhibition at a concentration of 1 mM of the inhibitor were determined at optimal pH, and at 35 °C. For G1 glucoamylase,[27] the percentages of inhibition observed for compounds **1**, **3**, and **4** were 23%, 39%, and 52%, respectively, while compound **2** showed no inhibition. Curiously, the fagomine homologue, with only three substituents,[9] displayed a 61% inhibition at a 1 mM concentration. For the A385T mutant of β-glucosidase from *Paenybacillus polymyxa*,[26] only the β-D-*manno*-like analogue (**3**) was able to inhibit this enzyme (72% inhibition at a 1 mM concentration, which corresponds to an IC_{50} of 350 μM). As will be shown in the following section, the predictions of the docking experiments perfectly match the observed inhibitions. We wish to emphasize the fact that the docking experiments were carried out before performing the inhibition assays.

Molecular Docking of Compounds 1−4 Towards Glycosidases

With all this information available, we decided to explore the atomic features of the interaction process. Therefore, molecular docking experiments of the two major conformations of each of the four compounds **1**−**4** in the binding site of three different glycosidases were performed to find the most favored conformation of these analogues in their binding state and to try to rationalize the observed inhibitory capacity of these molecules. They are indeed able to interact with different enzymes, even when they show different relative stereochemistries to those of the compounds targeted by the enzymes.

Thus, the two main low energy conformers of the four monosaccharide analogues **1**−**4** in solution were docked in the binding site of α-galactosidase from rice[25] (family GH27, with a β/α_8 fold, and two Asp catalytic residues, Asp185 and Asp130) as an analogue of *A. niger* α-galactosidase, glucoamylase from *A. awamori* var. X-100[26] (family GH15, with a α/α_6 fold, and two Glu catalytic residues, Glu179 and Glu400), and β-glucosidase A from *B. polymyxa*[27] (family GH1, with a β/α_8 fold, and two Glu catalytic residues Glu166, Glu352) using AutoDock 3.0. These enzymes were chosen since their crystallographic structures (see Table 8) with some inhibitors have been published. Furthermore, they belong to the same families and therefore may resemble the features of some of the enzymes whose inhibition features by **1**−**4** have been studied.

Table 8. Details of the enzyme X-ray crystal structures

Enzyme	PDB Code	EC Number	Resolution (Å)	Reference
α-Galactosidase from rice	1UAS	3.2.1.22	1.50	[25]
Glucoamylase from *A. awamori* var. X100	1DOG	3.2.1.3	2.40	[26]
β-Glucosidase A from *B. polymyxa*	1BGG	3.2.1.21	2.30	[27]

Validation of the Docking Method

To ensure that the ligand orientations and positions obtained from the docking studies were likely to represent valid and reasonable potential binding modes of the inhibitors, the docking parameters were first validated for each crystal structure used.[25−27] Each ligand found in the crystal structure of the enzyme−inhibitor complexes was docked into its corresponding enzyme and the AutoDock results were compared with the X-ray ones. The results for the validation method are given in Table 9. The low number of structures found for each cluster suggests that several independent docking runs can be conducted with ease, as performed here, to allow the minimization protocol to find a true energy minimum. Thus, the root mean square deviations (RMSD) for the lowest energy member indicate that the docking parameters can successfully predict the positions of the natural ligands, especially of D-galactose.

Table 9. Docking details of the natural ligands

Protein	Ligand	Cluster (structures)	RMSD
α-Galactosidase, rice	D-Galactose[25]	1 (1)	0.75
Glucoamylase, *A. awamori* var. X100	1-Deoxynojirimycin[26]	1 (2)	1.45
β-Glucosidase A, *B. polymyxa*	Gluconic acid[27]	1 (7)	1.12
		2 (5)	1.08

Docking of Compounds 1−4 in α-Galactosidase from Rice, as a Model of Coffee Bean α-Galactosidase

After energy minimizations with the AMBER* force field, all protonated structures maintained the initial geometry, referred to as **A**, **B** or **C**. The results of docked monosaccharide analogues in the binding site of α-galactosidase from rice are listed in Table 10. The type of conformation (**A**, **B** or **C**) is given next to the compound code. The results of the inhibition studies of α-galactosidase from coffee beans are also included.[9] All the compounds **1**−**4** were found to occupy the same binding site as D-galactose within α-galactosidase. The different conformers can bind in approximately the same region of the enzyme, with conformer **1A** having the most favorable interaction energy with the enzyme (see Table 10), being more favorable than

Table 10. Docking of monosaccharide analogues in the binding site of α-galactosidase from rice[25]

Comp. conformer	Cluster (structures)	Docked energy[a]	$\Delta G_{binding}$	Intermolec. energy	Internal energy of ligand	% Inhibition[b] (coffee beans)
1A	1 (1)	–8.10	–7.77	–8.08	–0.02	98
1B	1 (1)	–7.98	–7.64	–7.95	–0.03	
2A	1 (4)	–7.77	–7.53	–7.84	+0.07	88
2C	1 (3)	–6.47	–6.19	–6.51	+0.03	
4A	1 (2)	–7.28	–7.38	–7.69	+0.41	74
4B	1 (2)	–7.29	–6.81	–7.12	–0.17	
3A	1 (1)	–7.42	–7.04	–7.35	–0.06	52
3B	1 (1)	–7.29	–7.12	–7.43	+0.15	

[a] All energies are in kcal·mol^{-1}. [b] At a concentration of 1 mM of inhibitor, optimal pH, see ref.[9]

conformer **1B** by about 0.5 kJ·mol^{-1}, which also binds to the enzyme better than any other conformer of the other compounds. As a key example, the conformation **1A** of the D-*gluco* analogue in the protein's binding site is shown in Figure 7.

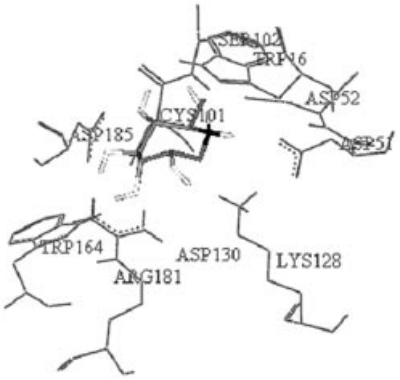

Figure 7. Docked structure of conformer **1A** of the D-*gluco* analogue in the binding site of α-galactosidase from rice[25]

The same amino acid residues involved in the binding of galactose are also involved in the proposed complexes of the different monosaccharide mimics. In the crystal,[25] Arg181, Trp164, as well as Asp185 formed hydrogen bonds with the O2 oxygen atom of galactose. Lys128 is hydrogen bonded to the two hydroxy oxygen atoms O3 and O4. Asp51 and Asp52 are hydrogen bonded to O4 and O6 atoms, respectively. In addition, a hydrophobic contact is observed for residue Trp16. The activity of **1A** as a galactose analogue can be explained by the replacement of the axial O4 of galactose by an axially oriented O3 in the **1A** conformer (Figure 7). Asp185 provides a bifurcated hydrogen bond to both O4 and O5, which adopt a pseudoequatorial orientation. Lys128, Arg181, Asp 51, and Asp52 are also involved in hydrogen bonding. Additionally, in this binding mode for **3**, the seven-membered ring of **1A** is surrounded by Trp16 and Trp164, a type of sugar–aromatic interaction seen in a variety of complexes between proteins and carbohydrates,[29] which is also present in the other two docking models (see below). Also, the additional stabilization found in this conformer is probably due to hydrogen bonding between one of the protons attached to the nitrogen and Asp51, a feature that only occurs for the **1A** conformer.

Most strikingly, a fairly good quantitative relationship is observed between the experimental percentage of enzyme inhibition and the estimated free energy of binding for all compounds (Figure 8). This good agreement indicates that the binding modes proposed are reasonable. Although these results should be taken with caution due to the different nature of the enzymes tested for inhibition and used for docking, it is tempting to try to rationalize the interaction on the basis of the 3D structure of the complex.

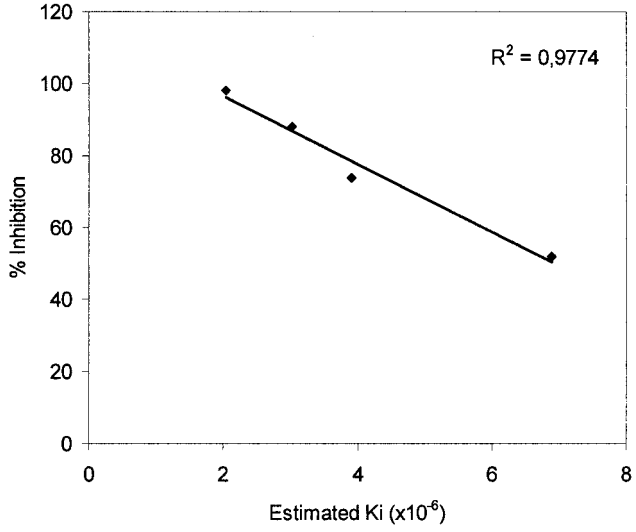

Figure 8. Relationship between the inhibition measured[9] for *A. niger* α-galactosidase and the estimated *Ki* (inhibition constant) (from the interaction binding energies) of **1**–**4** for α-galactosidase of rice; the measured inhibition versus the free energy of binding also showed a fairly good correlation (r^2 = 0.985)

Glucoamylase from A. awamori

The results of the docking protocol for the binding of **1**–**4** to the glucoamylase from *A. Awamori* are summarized in Table 11. The X-ray structure of this enzyme presents its complex with 1-deoxynojirimycin.[26] Residues that provide hydrogen bonding to 1-deoxynojirimycin are Asp55, Arg305, and Arg54. Besides, Glu179 is the catalytic acid and Glu400 is the catalytic base. The available biological data concerning inhibition[9] with *A. Niger* and G1 glucoamylase (this work) are also included in the same table. It can be observed that the inhibition profile for both enzymes is similar.

Table 11. Docking of monosaccharide analogues in the binding site[26] of glucoamylase from *A. awamori*

Conformer	Cluster (structures)	Docked energy[a]	$\Delta G_{binding}$	% Inhibition[b] (G1 glucoamylase	% Inhibition[b] (*A. niger*)
1A	1 (8)	–9.33	–9.12	24	NI
1B	1 (3)	–9.73	–9.32		
2A	1 (1)	–9.35	–8.98		NI
	3 (10)	–9.14	–8.88		
2C	1 (7)	–9.62	–9.28	NI	
	2 (14)	–9.43	–8.95		
4A	1 (2)	–9.21	–9.02		45
4B	1 (9)	–9.83	–9.61	52	
3A	1 (6)	–9.64	–9.19		34
3B	1 (7)	–9.49	–9.36	39	

In all cases, the docking protocol again leads to a binding mode fairly similar to that present in the crystal structure, with a perfect superimposition between 1-deoxynojirimycin and the glycomimetics. The residues mentioned above are interact similarly with the different glycomimetics. However, in this case, the best binding energy is provided by the α-L-*gulo*-like compound **4** in the **4B** conformation. The structure of **4B** docked in the enzyme's binding site is depicted in Figure 9 (a). Apart from hydrogen bonding involving Asp55, Arg305, Arg54, Glu179, and Glu400, there are also interactions with several aromatic residues (Tyr48, Trp52, Trp178, Trp317, and Trp417) that further stabilize **4B**. There is a fairly good superimposition with 1-deoxynojirimycin in the X-ray complex,[26] and since only O3 of **4B** adopts a pseudoaxial orientation, the rest of the hydroxy groups may resemble the D-*gluco*-type configuration. Again, there is a very good correlation between docked energies, binding energies, and the inhibition data (Table 11).[9] The compounds that provided no inhibition or weak inhibition to both enzymes are those that have the worst binding energies. The data suggest that compound **4** will be bound in a **B**-type conformation. The relative docked energies of α-L-*gulo*, **4B**, and β-D-*manno*, **3A**, analogues agree with the experimental relative inhibition of the two glucoamylases.[9]

β-Glucosidase A from *B. polymyxa*

The results of these docking experiments and the inhibition data (for β-glucosidases from almonds[9] and *B. Polymyxa*, this work) are summarized in Table 12. The best docking and binding affinity is provided by conformation **3B** of the β-D-*manno*-like analogue, as depicted in Figure 9 (b).

Again, the docking results predict that the monosaccharide analogues occupy the same binding site as the natural acyclic gluconic acid, as observed for the perfect superimposition for **3B** and the ligand in the crystallographic dataset[27] [Figure 9 (b)]. In the crystal structure, hydrogen bonding to the ligand is provided by Gln20, His121, Glu405, and the two catalytic residues, Glu166 and Glu352. For all compounds, the conformation with the lowest docking energy is the one that predominates in free solution, with the exception of compound **2**. Strikingly, only the compound with the best docking energy (compound **3**) is able to inhibit *B. polymyxa*, while the best docking energies (*manno* **3** and *gulo* **4**) correlate well with the inhibition of

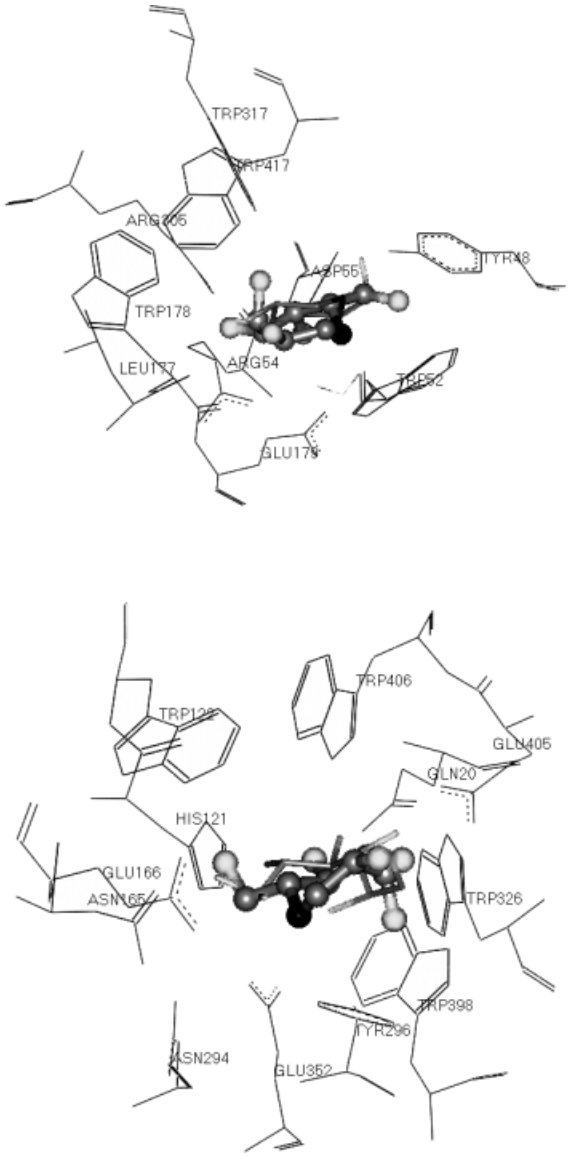

Figure 9. (a) The **4B** conformation of the α-L-*gulo*-like compound in the binding pocket of the glucoamylase from *A. awamori*;[26] only O3 adopts a pseudoaxial orientation; (b) the **3B** conformation of the β-D-*manno*-like compound in the binding pocket of the β-glucosidase A from *B. polymyxa*;[27] only O3 adopts a pseudoaxial orientation; monosaccharide analogues are represented as ball and stick models, and the ligands in the X-ray structure [deoxynojirimycin[26] in (a) and gluconic acid[27] in (b)] as stick models; hydrogen atoms have been removed for clarity

Table 12. Docking of monosaccharide glycomimetics in the binding site of β-glucosidase A from *B. polymyxa* [27]

Conformer	Cluster (structures)	Docked energy[a]	$\Delta G_{binding}$[a]	% Inhibition[b] (*B. polymyxa*)	% Inhibition[b] (almonds)
1A	1 (15)	–10.09	–10.05	NI	NI
1B	1 (57)	–10.87	–10.55		
2A	1 (13)	–10.32	–9.94	NI	
	2 (45)	–10.24			NI
2C	1 (7)	–9.83	–9.46		
	2(35)	–9.68	–9.42		
4A	1 (22)	–10.22	–9.95	NI	39
4B	1 (58)	–10.74	–10.28		
3A	1 (16)	–10.23	–9.99	72	62
3B	1 (44)	–11.39	–11.11		

[a] All energies are in kcal·mol^{-1}. [b] At a concentration of 1 mM of inhibitor, optimal pH, see ref.[9] NI: unmeasurable inhibition.

β-glucosidase from almonds. Therefore, the binding mode shown in Figure 9 (b) may be taken as an indication of the binding of these monosaccharide analogues. In the docking complex, all the residues involved in hydrogen bonding to gluconic acid in the crystal, Asn165 and Asn294 interact with the ligand, which is in turn surrounded by Tyr296, and four Trp residues, Trp122, Trp326, Trp398, and Trp406. The almost equatorial orientation of the substituents of **3B** (except for O3) provides a good match for the required glucose shape that this glucosidase is able to hydrolyse.

Conclusions

These polyhydroxyazepan glycomimetics **1**–**4** may adopt two conformations in solution which display some selectivity towards different glycosidases. On this basis, they have been docked in the binding sites of three selected enzymes whose X-ray coordinates are available. These enzymes, which belong to the same family as those used in the inhibition assays, served as models to predict the actual conformation of the analogues in the binding state. In all cases a strikingly good correlation was observed between the docked energies of the models and the percentages of inhibition of the tested enzymes. Although with the α-galactosidase from rice, the preferred conformation of the best analogue in the bound state is the less favored one in solution (although there is still selectivity with respect to the other analogues), for the other two chosen enzymes, glucoamylase from *A. awamori* and β-glucosidase A from *B. polymyxa*, the preferred conformer for binding is the one which is more populated in solution. According to our results, this protocol may be used to understand the inhibition ability of glycomimetics. Further studies in our laboratories are aimed at the design of novel analogues with enhanced inhibitory potency.

Acknowledgments

We would like to thank the European Community's Human Potential Programme (under contract HPRN-CT-2002–00173), the DGICYT of Spain (Grant BQU2003–03550-C03–01) and the Swiss National Science Foundation for financial support. We also thank the Ecole Normale Supérieure for the short stay of J.J.-B. in Paris. K.M.-M. and J.L.M.-F. thank CONACYT and the Universidad Nacional Autónoma (México) for a travel grant. We are indebted to Dr. Z. Fujimoto (Tsukuba, Japan) for providing the X-ray coordinates of rice α-galactosidase prior to availability and to Dr. A. Olson (Scripps Research Institute, USA) for providing AutoDock and auxiliary programs. We also thank Dr. J. Sanz-Aparicio (Madrid, Spain) and Dr. B. Svensson (Carlsberg Laboratory, Denmark) for samples of *B. polymyxa* glucosidase and G1 glucoamylase, respectively.

[1] [1a] V. H. Lillelund, H. H. Jensen, X. Liang, M. Bols, *Chem. Rev.* **2002**, *102*, 515–553. [1b] O. R. Martin, P. Compain, *Curr. Top. Med. Chem.* **2003**, *3*, i–iv.
[2] A. Mitrakou, N. Tountas, A. E. Raptis, R. J. Bauer, H. Schulz, S. A. Raptis, *Diab. Med.* **1998**, *15*, 657.
[3] T. D. Butters, R. A. Dwek, F. M. Platt, *Curr. Top. Med. Chem.* **2003**, *3*, 561–574.
[4] [4a] J. E. Groopman, *Rev. Infect. Dis.* **1990**, *12*, 908–911. [4b] G. S. Jacob, *Curr. Opin. Struct. Biol.* **1995**, *5*, 605–611 and references cited therein. [4c] M.-J. Papandreou, R. Barbouche, R. Guieu, M. P. Kieny, E. Fenouillet, *Mol. Pharmacol.* **2002**, *61*, 186–193.
[5] [5a] S-F. Wu, C.-J. Li, C.-L. Liao, R. A. Dwek, N. Zitzmann, Y.-L. Lin, *J. Virology* **2002**, *76*, 3596–3604 and references cited therein. [5b] A. Mehta, S. Ouzounov, R. Jordan, E. Simsek, X. Y. Lu, R. M. Moriarty, G. Jacob, R. A. Dwek, T. M. Block, *Antiviral Res.* **2003**, *57*, 56. [5c] P. Greimel, J. Spreitz, A. E. Stütz, T. M. Wrodnigg, *Curr. Top. Med. Chem.* **2003**, *3*, 513–523.
[6] [6a] S. L. White, T. Nagai, S. K. Akiyama, E. J. Reeves, K. Grzegorzewski, K. Olden, *Cancer Commun.* **1991**, *3*, 83–91. [6b] P. E. Goss, J. Baptiste, B. Fernandes, M. Baker, J. W. Dennis, *Cancer Res.* **1994**, *54*, 1450–1457. [6c] P. D. Rye, N. V. Bovin, E. Vaslova, R. A. Walker, *Glycobiology* **1995**, *5*, 385–389. [6d] A. D. Elbein, R. D. Molyneux, in *Imino Sugars as Glycosidase Inhibitors: Nojirimycin and Beyond* (Ed.: A. E. Stütz), Wiley-VCH, Weinheim, **1999**, chapter 11, pp. 216–251. [6e]N. Zitzmann, A. S. Mehta, S. Carrouée, T. D. Butters, F. M. Platt, J. McCauley, B. S. Blumberg, R. A. Dwek, T. M. Block, *PNAS* **1999**, *96*, 11878–11882. [6f] N. Asano, *J. Enzyme Inhibition* **2000**, *15*, 215–234.
[7] [7a] T. D. Heightman, A. T. Vasella, *Angew. Chem. Int. Ed.* **1999**, *38*, 750–770. [7b] A. Vasella, G. J. Davies, M. Böhm, *Curr. Opin. Chem. Biol.* **2002**, *6*, 619–629.
[8] J. Alper, *Science* **2001**, *291*, 2338–2343.
[9] H. Li, Y. Blériot, C. Chantereau, J.-M. Mallet, M. Sollogoub, Y. Zhang, E. Rodríguez-García, P. Vogel, J. Jiménez-Barbero, P. Sinaÿ, *Org. Biomol. Chem.* **2004**, *2*, 1492–1499.

[10] T. Weimar, R. Woods, in *NMR spectroscopy of glycoconjugates* (Eds.: J. Jiménez-Barbero, T. Peters), Wiley-VCH, Weinheim, **2002**.
[11] M. Meyer, B. Meyer, *Angew. Chem.* **1999**, *111*, 1902−1906; *Angew. Chem. Int. Ed.* **1999**, *38*, 1784−1788.
[12] For the first applications of TRNOE in sugar−protein interactions, see: [12a] V. L. Bevilacqua, D. S. Thomson, J. H. Prestegard, *Biochemistry* **1990**, *29*, 5529−5537. [12b] V. L. Bevilacqua, Y. Kim, J. H. Prestegard, *Biochemistry* **1992**, *31*, 9339−9349. For a detailed rigorous analysis of TRNOE cross peaks, see: [12c] P. L. Jackson, H. N. Moseley, N. R. Krishna, *J. Magn. Reson., Ser. B* **1995**, *107*, 289−292. For recent applications, see also ref.[15].
[13] For applications of molecular docking protocols to glycosidase enzymes, see, for example: [13a] A. Laederach, M. K. Dowd, P. M. Coutinho, P. J. Reilly, *Proteins* **1999**, *37*, 166−175. [13b] J. K. Choi, B. H. Lee, C. H. Chae, W. Shin, *Proteins* **2004**, *55*, 22−33.
[14] For information on families of glycosidases, see: P. M. Coutinho, B. Henrissat, *Carbohydrate-Active Enzymes*, **1999**; on the internet see http://afmb.cnrs-mrs.fr/CAZY/index.html
[15] For applications of NMR to glycostructures, see: *NMR spectroscopy of glycoconjugates* (Eds.: J. Jiménez-Barbero, T. Peters), Wiley-VCH, Weinheim, **2002**.
[16] K. Stott, J. Stonehouse, J. Keeler, T.-L. Hwang, A. J. Shaka, *J. Am. Chem. Soc.* **1995**, *117*, 4199−4200.
[17] For a discussion on the application of molecular mechanics force fields to sugar molecules, see: S. Pérez, A. Imberty, S. B. Engelsen, J. Gruza, K. Mazeau, J. Jiménez-Barbero, A. Poveda, J. F. Espinosa, B. P. van Eijck, G. Johnson, A. D. French, M. L. C. E. Kouwijzer, P. D. J. Grootenhuis, A. Bernardi, L. Raimondi, H. Senderowitz, V. Durier, G. Vergoten, K. Rasmussen, *Carbohydr. Res.* **1998**, *314*, 141−155.
[18] F. Mohamadi, N. G. J. Richards, W. C. Guida, R. Liskamp, M. Lipton, C. Caufield, G. Chang, T. Hendrickson, W.C. Still, *J. Comput. Chem.* **1990**, *11*, 440−467.
[19] S. W. Homans, *Biochemistry* **1990**, *29*, 9110−9118.
[20] N. L. Allinger, Y. H. Yuh, J. H. Lii, *J. Am. Chem. Soc.* **1989**, *111*, 8551−8559.
[21] W. C. Still, A. Tempzyk, R. Hawley, T. Hendrickson, *J. Am. Chem. Soc.* **1990**, *112*, 6127−6129.
[22] C. A. G. Haasnoot, F. A. A. M. de Leeuw, C. Altona, *Tetrahedron* **1980**, *36*, 2783−2793.
[23] A. Poveda, J. L. Asensio, M. Martín-Pastor, J. Jimenez-Barbero, *J. Biomol. NMR* **1997**, *10*, 29−43.
[24] G. M. Morris, D. S. Goodsell, R. S. Halliday, R. Huey, W. E. Hart, R. K. Belew, A. J. Olson, *J. Comput. Chem.* **1998**, *19*, 1639.
[25] Z. Fujimoto, S. Kaneko, M. Momma, H. Kobayashi, H. Mizuno, *J. Biol. Chem.* **2003**, *278*, 313.
[26] E. M. Harris, A. E. Aleshin, L. M. Firsov, R. B. Honzatko, *Biochemistry* **1993**, *32*, 1618.
[27] J. Sanz-Aparicio, J. A. Hermoso, M. Martinez-Ripoll, J. L. Lequerica, J. Polaina, *J. Mol. Biol.* **1998**, *275*, 491.
[28] K. Bock, J. O. Duus, *J. Carbohydr. Chem.* **1994**, *13*, 513−543.
[29] See, for example: [29a] M. Muraki, *Protein Pept. Lett.* **2002**, *9*, 195−209. [29b] H. Kogelberg, D. Solís, J. Jiménez-Barbero, *Curr. Opin. Struct. Biol.* **2003**, *13*, 646−653, and references cited therein.

Received May 7, 2004

